ISSN 1069-3513, Izvestiya, Physics of the Solid Earth, 2010, Vol. 46, No. 12, pp. 1080–1094. © Pleiades Publishing, Ltd., 2010.
Original Russian Text © A.I. Koptev, A.V. Ershov, 2010, published in Fizika Zemli, 2010, No. 12, pp. 66–81.

The Role of the Gravitational Potential of the Lithosphere in the Formation of a Global Stress Field

A. I. Koptev and A. V. Ershov

Geological Faculty, Moscow State University, Moscow, Russia

e-mail: koptev06@mail.ru

Received May 6, 2009

Abstract—The global stress field appearing in the Earth's lithosphere under the action of forces caused by the difference of gravitational potential is calculated. An original algorithm is proposed and the operational Earth Stresses program code is developed. The data on the topography, thickness, and density of the Earth's crust and the upper mantle, as well as the gravitational anomalies and thermal conditions in the lithosphere were taken into account in the calculations. A comparison of the calculation results and the observed data makes it possible to conclude that the action of the forces of the difference of the gravitational potential alone is sufficient to explain the features of the first order of the stress field in the Earth's lithosphere.

DOI: 10.1134/S1069351310120050

INTRODUCTION

The stress sources in the Earth's lithosphere are the same forces as those that make the lithosphere's plates move. The interpretation of the nature of these forces has changed with time. The early models of the tectonics of the lithosphere's plates showed that the main reason for the movement of the lithosphere's plates is the mantle convection that acted on the lithosphere's plates due to the forces of viscous cohesion at the lithosphere-astenosphere interface [Ueda, 1980].

Then, the idea occurred that the source of the movement of the plates could lie within them. The variations of the thickness of crustal layers and density inhomogeneities, appearing due to the heterogeneity of the thermal conditions and composition, determine the generation of forces that tend to destroy these inhomogeneities and lead the system to a more homogeneous state, which is characterized by smaller values of potential energy. These forces include the so-called ridge push force that is specified by the thermal inhomogeneity under the middle of the ridges, the force of the gravitational spreading of the thickened crust of mountain belts, the force of spreading in the areas of thermal arches, etc. The procedure for quantitatively estimating the force as the difference of the vertical integrals of lithostatic pressure in laterally situated columns was supposed in the works [Frank, 1972; Artyushkov, 1973]. In addition, the plate undergoes the action of a so-called slab pull forces that appears due to the gravitational instability of a rather cold and consequently denser oceanic lithosphere of the subsiding plate [Forsyth, Ueda, 1975].

The relations between these two types of forces of a "self-moving" lithosphere were differently estimated in quantitative models by J. Harper [Harper, 1975], who supposed that the slab pull forces considerably exceed the ridge push force, and by D. Forsyth and S. Uyeda [Forsyth and Uyeda, 1975], who believed that the force of negative slab buoyancy is practically balanced by the forces of resistance from the enclosing mantle.

The first global models of the stress field in the Earth's lithosphere were calculated by R. Richardson et al. [Richardson et al., 1975; 1976; 1979]. These works showed that the model stress field is well consistent with the observed one if slab pull forces and ridge push force are comparable. The influence of mantle convection was assumed to be purely passive: the mantle forces acted only as resistance forces directed against the plate movement, thus providing the required balance of forces and moments.

Later the regional stress fields were calculated for large single regions in the Earth: Indo-Australian plate [Sandiford et al., 1995; Coblentz et al., 1995; 1998; Reynolds et al., 2002], Australian plate [Burbidge, 2004], North-American plate [Richardson, Reding, 1991; Liu and Bird, 1998; Flesh et al., 2000], South-American plate [Coblentz and Richardson, 1996; Meijer et al., 1997], African plate [Coblentz and Sandiford, 1994], New Zealand [Liu and Bird, 2002], Phillippine Sea [Pacanovsky, 1999], etc.

In these models, except for the works by S. Reynolds et al. [Reynolds, et al., 2002], D. Burbidge [Burbidge, 2004], and Z. Liu and P. Bird [Liu and Bird, 2002], the elastic rheological model was used, the lithosphere's thickness was assumed constant, and the conformance evaluation between the calculated and observed data was only qualitative. The stress field was assumed to appear due to the action of forces applied to the boundaries of the modeled region. These interface forces were selected based on the best conformance of the calculated stress field to the observed data and were interpreted as the ridge push force or the slab pull forces; the mantle forces were assumed passive as in the case of the above global models [Sandiford et al., 1995; Coblentz et al., 1995; 1998;

Coblentz, Sandiford, 1994]. The works by Burbidge [Burbidge, 2004] and Liu and Bird [Liu and Bird, 2002] are different in these terms, as their models assigned rates of movement on the plate's interface as boundary conditions.

As a result of these works aimed at determining the relative role of different moving forces of plate tectonics in the formation of a regional stress field, it was established that this role of the slab pull forces and the forces of mantle convection is rather small and that topographical forces, i.e., the ridge push forces and the forces of gravitational spreading of continents, determine the stress field. Only Reynolds et al. [Reynolds et al., 2002] calculated a set of variants, performed the quantitative correlation of the calculation data with the observations, and made the opposite conclusion about the significant influence exerted on the observed stress state also by the subduction forces.

When comparing the above works, we should mention the evident advantage of the models by Burbidge [2004] and Liu and Bird [2002] who allowed for thermal lithosphere conditions (at laterally constant thermal-physical properties of the lithosphere) and discontinuous failures in their calculations, quantitatively determined the bottom of the lithosphere on the principle of local isostasy, and included the inelastic behavior of the lithosphere in their model. They estimated the role not only of the ridge push forces and the slab pull forces, but also the forces of mantle flows. Here, in one case, the influence of the latter forces was acknowledged to be insignificant [Liu and Bird, 2002], in the other case, the model was highly sensitive to boundary conditions related to forces acting on the bottom of the lithosphere [Burbidge, 2004]. The correspondence of the model to the observations was checked based on the quantitative closeness of the calculated and observed orientations of the principal axes of stresses (by seismological, geological, and well data), rates of plate movement (by geodetic data), and rates of movement along faults (by geological data). Using quantitative analysis, the authors established that there is no combination of boundary conditions that could provide the satisfactory convergence for all types of the compared data.

Some other approach was used in the works [Galybin and Mukhamediev, 1999; Mukhamediev, 2000; Mukhamediev and Galybin, 2001; Mukhamediev, et al., 2006]. A regional stress field was calculated based on the available measurements of stresses *in situ* by directly integrating the equations of elasticity theory at the assigned field of the trajectories of the principal stresses or using a special form of analysis of a non-classical boundary problem of elasticity theory. An obvious advantage of this approach is that the calculated stress field fully coincides with the actual data (this is a direct consequence of the selected calculation procedure).

However, the approach itself to modeling a regional field of stresses has one major disadvantage. If we try to compare the models considered the best by the authors, we see that the boundary forces applied on the common boundary of the plates but calculated in the different models considerably differ. Thus, in global terms, these models are not mutually consistent.

The modern global models of the stress state in the Earth's lithosphere were made by Bird [Bird, 1998], K. Lithgow-Bertelloni and J. Guynn [Lithgow-Bertelloni and Guynn, 2004]. Both works come to a common conclusion that the calculated field corresponds best to the observed field if the model comprises the mantle forces; while only topographical forces (forces that are caused by the difference of gravitational potential) were unable to form a reliable distribution of stresses.

From this it follows that the present stage of investigations into this problem shows a contradiction between the results of the global and regional modeling of the stress field of the Earth's lithosphere. The majority of regional models prove that the use of only topographical forces is enough to explain the existing stress state within the admissible accuracy, whereas the global models show that mantle and subduction forces must also be taken into account.

To solve this contradiction, we modeled the global stress field in this work regardless of the action of mantle forces and slab pull forces, but made the qualitative calculation of gravitational potential more detailed than in the works [Bird, 1998] and [Lithgow-Bertelloni and Guynn, 2004]. It was estimated not only by topography (a digital ETOPO5 relief model) and structural-substantial composition of the Earth's crust (by the data of CRUST 2.0 model [Bassin et al., 2000; Mooney et al., 1998]) but also with respect to gravitational anomalies (a gravitational EGM96 model [Lemoine et al., 1998]) and the nonlinear model of a thermal lithosphere structure that consisted of the actual data on the distribution of annual average temperatures on the Earth's surface [Leemans et al., 1991; Lieth et al., 1972].

1. PROCEDURE FOR THE CALCULATION OF A TWO-DIMENSIONAL STRESS FIELD

The stress field σ_{ij} in the Earth's lithosphere was calculated by the numerical solution of the equilibrium equation

$$\sum_{i=1}^{3} \frac{\partial \sigma_{ij}}{\partial x_i} + F_j = 0 \qquad (1)$$

for a spherical shell with cuts and rheological properties changing in space and for the assigned field of external forces F_i (calculated from the difference of the lithosphere gravitational potential, see 1.6).

Suppose the lithosphere's rheology is elasto-plastic. Assume that the total strain ε_{ij} is the sum of the elastic ε_{ij}^e and inelastic ε_{ij}^r parts:

$$\varepsilon_{ij} = \varepsilon_{ij}^e + \varepsilon_{ij}^r. \qquad (2)$$

The stresses are related to the elastic strain by Hooke's law for an isotropic medium:

$$\sigma_{ij} = \lambda \sum_{k=1}^{3} \delta_{ij} \varepsilon_{kk}^{e} + 2\mu \varepsilon_{ij}^{e}, \quad (3)$$

with Lame coefficients (λ, μ) that change depending on the power, composition, structure, and temperature state of the lithosphere.

Calculate the plasticity based on the flow theory. Use the associated law of plastic flow to determine the connection between the stress tensor and tensor of increments of plastic strain (and the tensor of the rates of plastic strains)

$$d\varepsilon_{ij}^{r} = h d\varepsilon_{ij} = h\frac{1}{E}((1+\nu)d\sigma_{ij} - \nu\delta_{ij}d\sigma_{kk}), \quad (4)$$

where E, ν is the Young modulus and the Poisson ratio,

$$h(\sigma'_{ij}) = \begin{cases} 0 & \text{at } \sigma'_{ij} < \sigma_{ij}^{cr} \\ 1 & \text{at } \sigma'_{ij} \geq \sigma_{ij}^{cr}, \end{cases} \quad (5)$$

where σ'_{ij} s the deviator of the stress tensor, and σ_{ij}^{cr} is the strength of the lithosphere. As a strength criterion we take the simplest type of this equation that corresponds to the degenerate strength criterion of a Mohr-Coulomb with a zero angle of internal friction and assigned cohesion ((σ_{ij}^{cr}).). Assume that the elastic modules are equal at elastic loading and plastic or elastic unloading. The plastic flow begins when the applied stresses exceed the assigned ultimate strength; it accommodates the total strain that exceeds the threshold value. Calculate the ultimate strength at each point of the shell using the real properties of the lithosphere (see 1.5).

Represent the strain tensor by displacements u_i in the usual way:

$$\varepsilon_{ij} = \frac{1}{2}\left(\frac{\partial u_i}{\partial x_j} + \frac{\partial u_j}{\partial x_i}\right). \quad (6)$$

The boundary conditions are the field of generalized topographical forces F_i and the stresses on the shell cuts (zero stresses or the ones depending on displacements of adjacent segments of the shell).

To solve equation (1) quantitatively, we use the method of final volumes with the explicit conservative numerical pattern in the Lagrangian coordinates. The calculated mesh covered the sphere with a radius of 6371 km and consisted of quadrangular cells.

Despite the fact that the problem under consideration is stationary and, consequently, its solution is time-independent, we used the explicit pattern in the calculations that assumed a solution of the equilibrium equation with a nonzero nonstationary term

$$\sum_{i=1}^{3} \frac{\partial \sigma_{ij}}{\partial x_i} + F_j + F_{\text{damp}}\left(\frac{\partial u_j}{\partial t}\right) = \rho g \frac{\partial^2 u_j}{\partial t^2}. \quad (7)$$

Find a stationery solution of this equation that is obtained due to the introduction of viscous damping forces F_{damp} that depend on the rate of medium displacement $\frac{\partial u_j}{\partial t}$ and tend to zero when these rates approach zero. The accelerations $\frac{\partial^2 u_j}{\partial t^2}$, that constitute the right part of the equation and the damping forces, tend to zero when the equilibrium state is reached, and, thus, the solution of equation (7) coincides with the solution of (1).

The length of the time interval of our calculations was determined by the condition of reaching a stationary state. The time step was chosen so that the numerical pattern was steady (see 1.2).

1.1 The Main Cycle of Calculations

During the calculations, we perform the cyclical recalculation of the displacement rates ($\dot{u}_i$) to the strain rates ($\dot{\varepsilon}_{ij}$), the strain rates ($\dot{\varepsilon}_{ij}$) to the stresses (σ_{ij}), the stresses (σ_{ij}) to the forces (F_i), and the forces (F_i) back to the displacement rates ($\dot{u}_i$). Part of these values (displacement rates ($\dot{u}_i$), and forces (F_i)) are centered in the nodes of the calculated mesh, and part of them (the strain rates (($\dot{\varepsilon}_{ij}$),) and the stresses (σ_{ij})), in the cells (Fig. 1).

Recalculate the displacement rates (($\dot{u}_i$)) to the strain rates (($\dot{\varepsilon}_{ij}$)) by formula

$$\dot{\varepsilon}_{ij} = \frac{1}{2}\left(\frac{\partial \dot{u}}{\partial x_j} + \frac{\partial \dot{u}_j}{\partial x_i}\right) \quad (8)$$

using Gauss' law (a theorem on gradient)

$$\left\langle \frac{\partial \dot{u}_i}{\partial x_j} \right\rangle \equiv \frac{1}{A}\int\int_A \frac{\partial \dot{u}_i}{\partial x_j} dA = \frac{1}{A}\oint_S n_j \dot{u}_i dS, \quad (9)$$

where,

$\left\langle \frac{\partial \dot{u}_i}{\partial x_j} \right\rangle$ is the mean average of the value $\frac{\partial \dot{u}_i}{\partial x_j}$ in the domain; A is the area of this domain; n_j is the vector of the external normal to the domain boundary.

The integral in the right part of the equation is taken with respect to the domain boundary.

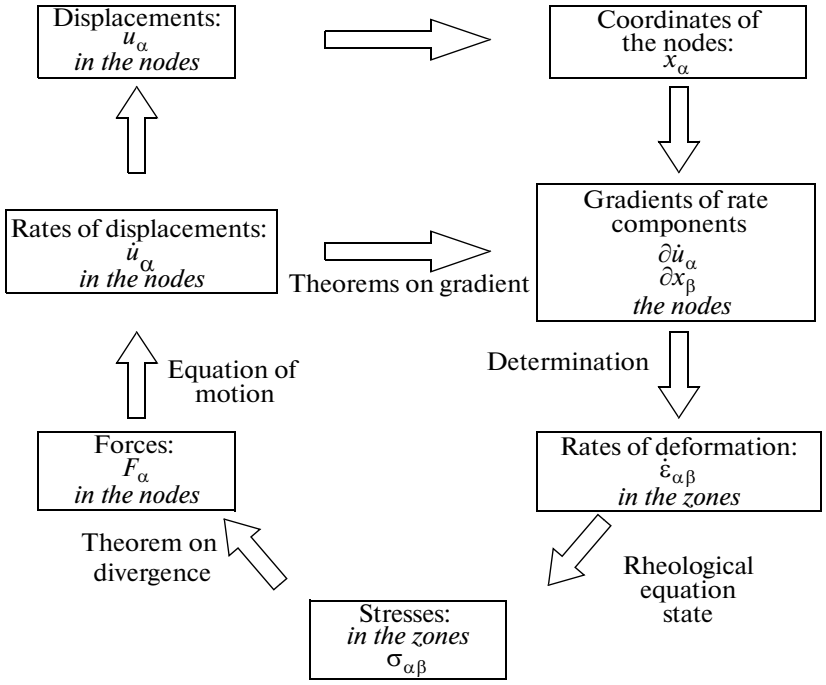

Fig. 1. General pattern of calculations.

Calculate the stresses (σ_{ij}) from the strain rates ($\dot{\varepsilon}_{ij}$) by Hooke's law:

$$\sigma_{ij}(t+dt) = \sigma_{ij}(t) + dt\left(\lambda \sum_{k=1}^{3} \delta_{ij}\dot{\varepsilon}_{kk} + 2\mu\dot{\varepsilon}_{ij}\right), \quad (10)$$

where δ_{ij} is the Kronecker symbol

$$\delta_{ij} = \begin{pmatrix} 1 & 0 & 0 \\ 0 & 1 & 0 \\ 0 & 0 & 1 \end{pmatrix}, \quad (11)$$

λ and μ are Lame coefficients expressed by the Young modulus (E) and the Poisson ratio (ν) as follows:

$$\lambda = \frac{E\nu}{(1+\nu)(1-2\nu)}, \qquad \mu = \frac{E}{2(1+\nu)}. \quad (12)$$

In the case of the flat-stress state determined by conditions

$$\sigma_{33} = \sigma_{23} = \sigma_{13} = 0, \quad (13)$$

equation (10) becomes

$$\sigma_{ij}(t+dt) = \sigma_{ij}(t) + dt\left(\lambda^* \sum_{k=1}^{2} \delta_{ij}\dot{\varepsilon}_{kk} + 2\mu\dot{\varepsilon}_{ij}\right), \quad (14)$$

where

$$\lambda^* = \lambda\left(1 - \frac{\lambda}{2\mu+\lambda}\right). \quad (15)$$

The stresses (σ_{ij}) centered in the cells are recalculated in the nodal forces using the theory on divergence for the domain A' shown in Fig. 2 from the formula

$$\iint_{A'} F_i dA' = \oint_S \sigma_{ik} n_k dS, \quad (16)$$

where F_i are the nodal forces and n_k is the vector of the external normal to the boundary of the domain A'. The right part of equation (16) implies summation by the repeating index k that possesses the values 1 and 2.

Introduce the external forces: boundary and generalized topographical forces (see 1.6) to the nodal forces obtained from (16).

The change in the nodal forces is found using Newton's second law:

$$\frac{\partial \dot{u}_i}{\partial t} = \frac{F_i + F_{\text{damp}}}{m}, \quad (17)$$

where m is the cell mass that was determined as the integral of the density ρ within the domain A' (Fig. 2) containing the respective node, and F_{damp} is the damping force. Due to the use of equation (17), elastic waves appear in the model; a damping force imitating the viscous dissipation of elastic energy is introduced for their damping.

The value of the damping force (F_{damp}) was chosen in the following way:

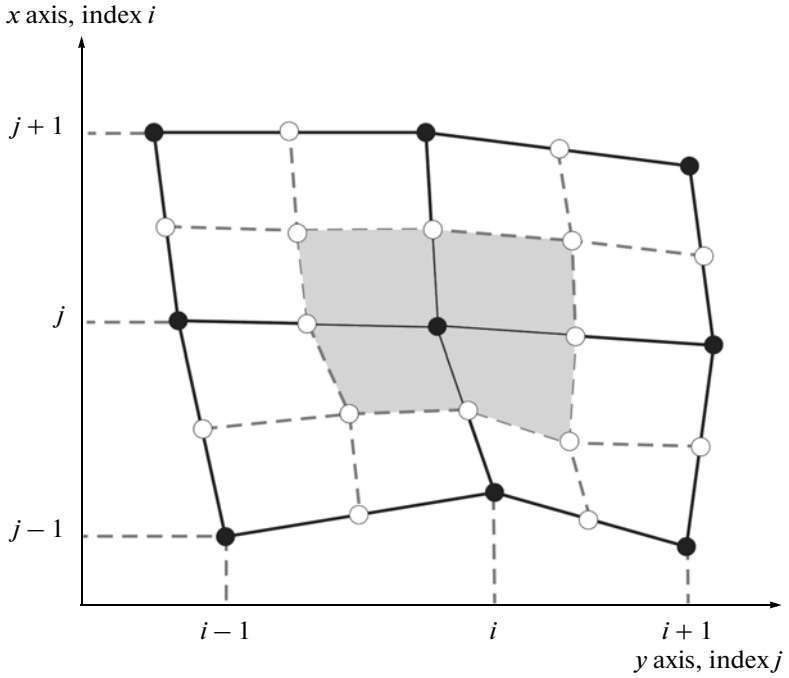

Fig. 2. Gray colored area is the domain A' over which the integration is done in formula (16).

$$F_{\text{damp}} = -0.5|F_i|\,\text{sgn}(\dot{u}_i), \tag{18}$$

where $\text{sgn}(\dot{u}_i)$ is the sign of the rate of displacement to the respective direction, i.e.,

$$F_{\text{dump}} = -0.5F_i, \quad \text{if } \dot{u}_i > 0; \tag{19a}$$

$$F_{\text{dump}} = 0.5F_i, \quad \text{if } \dot{u}_i < 0. \tag{19b}$$

We should mention that the value and the direction selected for the damping force does not influence the final distributions of stresses and other calculated values (since this force is proportional to the acceleration u_i, and the values u_i tend to zero when approaching the equilibrium state), but influences only the rate at which the equilibrium state is reached by the model [Poliakov et al., 1993].

The nodal displacements (u_i) are calculated from the rates of displacements ($\dot{u}_i$) at every time step

$$u_i(t + dt) = u_i(t) + \dot{u}_i dt. \tag{20}$$

As initial conditions of the model, we used zero displacements, rates of displacements, and stresses.

The above-described cycle of calculations was repeated until the equilibrium state was reached, i.e., the state when all nodal forces are in equilibrium. As a criterion for this state, we used the condition that the assigned threshold value should not be exceeded by the nodal forces.

Despite the fact that the evolution of the system in time is estimated during the calculation of a pure elastic problem, strictly speaking, we are interested only in its finite steady state.

We perform elasto-plastic calculations the following way. First, we estimate the equilibrium stress field within the pure elastic model at the assigned configuration of tectonic and boundary forces. Then, we add plasticity and calculate the stress field within the elasto-plastic model.

During the calculations we used the strength criterion to fulfill the condition that the main components of the stress deviator do not exceed the lithosphere's compression and tension strengths calculated by the procedure presented below (see 1.5).

1.2. Selection of the Time Step Parameter

The stability of the explicit pattern used depends on the time step that is selected so that the signal at one step is not propagated further than one cell. The maximum rate of signal propagation in the elastic medium, i.e., the propagation rate of a longitudinal sound wave is

$$V_p = \sqrt{\frac{K + \frac{4}{3}G}{\rho}}, \tag{21}$$

where V_p is the propagation rate of longitudinal waves, K is the volume modulus, G is the shear modulus, and ρ is the density. Thus, the time step is determined by the relation:

$$\delta t < \frac{\delta l}{V_p} = \delta l \sqrt{\frac{\rho}{K + \frac{4}{3}G}}, \tag{22}$$

where δl is the shortest distance in the cell. It can be estimated as the ratio of twice the area of the triangular zone to the length of its longest side, considering that the area of a triangle equals half of the product by height, and the shortest of the three heights is the shortest distance in the triangle:

$$\delta l = \frac{2A}{S_{\max}}, \tag{23}$$

where A is the area of the triangle and $S_{\max}$ is the length of its longest side.

We represent the volume modulus K and the shear modulus G by Lame coefficients as

$$K = \lambda + \frac{2}{3}\mu; \tag{24a}$$

$$G = \mu. \tag{24b}$$

From (22), (23), and (24), we have

$$\delta t < \frac{\delta l}{V_p} = \frac{2A}{S_{\max}}\sqrt{\frac{\rho}{\lambda + 2\mu}}. \tag{25}$$

1.3. Geometry of the Calculated Mesh

We assign the calculated mesh on a sphere whose cells have a quadrilateral shape, except for those adjacent to the triangular poles. As we know (for example [Polyakov et al., 1993]) unphysical zero-point energy modes of element deformation appear in quadrilateral cells during the linear parametrization of the strain (sand-glass modes). To eliminate this effect, we partition the rectangular cells into triangular ones, and calculate the zonal values separately for each triangular zone. There were two alternative partitions (Fig. 3). The result was averaged for the quadrilateral cell.

The sphericity of the calculated mesh is considered in the following way. The values centered in the nodes are calculated in the local plane coordinate system where the xy plane is tangential to the sphere in this node; and the values centered in the cells are found in the coordinate system whose xy plane is tangential in the cell center. In both cases, the x axis is oriented in parallels to the east, the y axis is directed in meridians to the north, and the z axis is directed radially from the center of the sphere.

The transformation of the local coordinate systems is the transformation of the $x'y'z'$ coordinate system with the center at the point with the coordinates λ' and φ' to the $x''y''z''$ coordinate system with the center at the point with the coordinates λ'' and φ'' (λ and φ are longitude and latitude, respectively). This transformation is made via the transition to the intermediate xyz coordinate system with the origin of the coordinates in the center of the sphere. The xy plane of this coordinate system lies in the plane of the equator (the x axis is directed towards the meridian that corresponds to latitude 0°, and the y axis, to 90°), the z axis coincides with the Earth's axis (passes through the Earth's poles) and is directed toward the North Pole (Fig. 4).

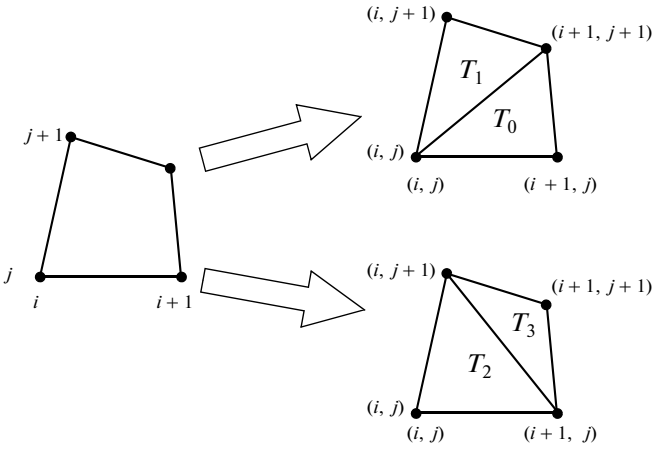

Fig. 3. Two alternative ways of dividing a quadrangular cell into a triangular zone.

We transform the $x'y'z'$ coordinate system to the xyz coordinate system by multiplying the transformed vector by the rotation matrix

$$\begin{pmatrix} x \\ y \\ z \end{pmatrix} = \begin{pmatrix} -\sin\lambda' & -\cos\lambda'\sin\varphi' & \cos\lambda'\cos(\varphi') \\ \cos\lambda' & -\sin\lambda'\sin\varphi' & \sin\lambda'\cos\varphi' \\ 0 & \cos\varphi' & \sin\varphi' \end{pmatrix} \begin{pmatrix} x' \\ y' \\ z' \end{pmatrix}. \tag{26}$$

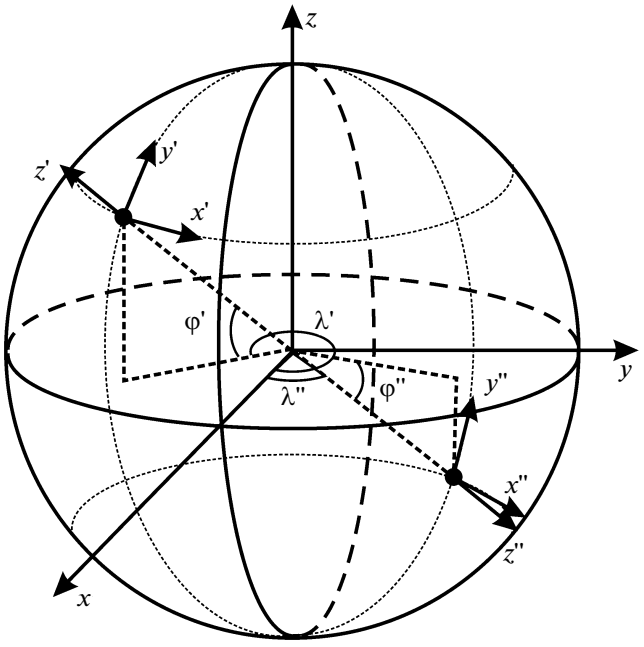

Fig. 4. Coordinate systems used for accounting for the sphericity of the calculated mesh.

The transformation

$$\begin{pmatrix} x'' \\ y'' \\ z'' \end{pmatrix} = \begin{pmatrix} -\sin\lambda'' & \cos\lambda'' & 0 \\ -\sin\varphi''\cos\lambda'' & -\sin\varphi''\sin\lambda'' & \cos\varphi'' \\ \cos\varphi''\cos\lambda'' & \cos\varphi''\sin\lambda'' & \sin\varphi'' \end{pmatrix} \begin{pmatrix} x \\ y \\ z \end{pmatrix} \quad (27)$$

enables us to pass from the xyz coordinate system to the $x''y''z''$ coordinate system.

The tensors are rotated similarly, but we used the following formula instead of matrix transformations:

$$p'_{kl} = \sum_{r=1}^{3}\sum_{s=1}^{3} \alpha_{kr}\alpha_{ls}p_{rs}, \quad (28)$$

where p'_{kl} is the current element of the tensor obtained during the recalculation; p is the initial tensor; α_{kr} and α_{ls} are the respective elements of the used rotation matrix [Kochin, 1965].

We neglect the Z component of vectors and tensors that appears in these recalculations.

In our calculation we changed the mesh geometry due to the shift of the mesh nodes. Therefore, at each step of the calculations, we checked its geometric correctness. We checked that the minimum length of the cell side ($S_{\min}$) was not less than $1/5\sqrt{A}$. If this condition was not fulfilled, we carried out a remeshing, i.e., generated a new mesh.

1.4. Consideration of Boundaries of Plates and Rupture Faults

The method allows "cutting" a mesh along the boundaries of cells. For nodes on the cutting line, we specially assigned a coefficient that showed the degree of influence exerted by cell-centered values (stresses, etc.) in the cells from the other side of the cut on the calculation of values centered in such nodes (displacement rates, forces, etc.). Thus, to calculate the balance of forces (16) for the nodes lying on the cut line, we take into account the contribution of those cells that lie on one side of the cut line, as well as the contribution of the cells on the other side of the cut, but multiplied by the assigned coefficient.

In the case this coefficient amounts to one in any cell, it means that the cut is absent in this place of the calculated mesh. If it is zero, the nodes that lie on the cut boundary and belong to the cells located on different sides of the cut can be displaced absolutely independently (the cells can either cross over or move apart). It is possible to impose a condition that the cell nodes could move only along the cut line.

The possibility to make calculations on a continuous mesh makes it possible to include lines of fractures and boundaries of a lithosphere's plates in the model. Changing the coefficient of interaction along the cut boundary, we can assign boundaries of different types on this section of the calculated mesh (zone of spreading, subduction, collision, etc).

1.5. The Calculation of a Lithosphere's Thickness and Rheological Properties

The stresses (σ_{ij}) that are calculated within the plane problem are in fact the quantities integrated with respect to the vertical coordinate:

$$\sigma_{ij}(x, y) = \int_0^{H_L} s_{ij}(x, y, z)dz, \quad (29)$$

where H_L is the lithosphere's thickness and s_{ij} is the stresses in the lithosphere.

The integral quantities are also elastic parameters of the lithosphere (Young modulus), with density (E, ρ):

$$E(x, y) = \int_0^{H_L} e(x, y, z)dz; \qquad \rho(x, y) = \int_0^{H_L} ro(x, y, z)dz, \quad (30)$$

where e and ro are the Young modulus and the density of rocks composing the lithosphere, respectively.

Assume that displacements, displacement rates, and strain rates are distributed uniformly along the vertical

$$u_i(z) = \text{const}; \quad \dot{u}_i(z) = \text{const}; \quad \dot{\varepsilon}_{ij}(z) = \text{const}. \quad (31)$$

The thickness and the thermal conditions of the lithosphere are calculated in the following way. Suppose that the lithosphere is in the state of local isostatic equilibrium. Therefore, the weights of any two vertical columns of the lithosphere from the surface to the depth of isostatic compensation must equal:

$$\int_{z_0(x_1, y_1)}^{z_l} ro(x_1, y_1, z_1)dz = \int_{z_0(x_2, y_2)}^{z_l} ro(x_2, y_2, z_2)dz, \quad (32)$$

where $z_0(x, y)$ is the absolute mark of the relief at the point with the coordinates (x, y), z_1 is the level of isostatic compensation, and the density ρ of the rocks composing the lithosphere at the assigned mineral composition depends on the temperature in the following way:

$$ro(T) = ro(T_0)(1 - \alpha(T - T_0)). \quad (33)$$

The distribution of temperature in the lithosphere is considered stationary and is calculated as

$$T(z) = T_0 + \int_{z_0}^{z} \frac{q(\zeta)}{k(\zeta)} d\zeta, \quad (34)$$

$$q(z) = q_0 - \int_{z_0}^{z} A(\zeta) d\zeta, \quad (35)$$

where T_0 is the temperature on the Earth's surface, $K(z)$ is thermal conductivity, and $q(z)$ is the heat flow, q_0 is the heat flow over the Earth's surface, and the volume heat-generation of the lithosphere's rocks $A(z)$ is taken to be exponentially decreasing with depth

$$A(z) = A_0 \exp\left(-\frac{z}{H}\right), \quad (36)$$

where A_0 and H are constants (3×10^{-6} W/s and 1×10^4 m, respectively).

The surface heat flow q_0 is not an independent input parameter of the model and is calculated based on the temperature on the bottom of the lithosphere $T(H_L)$, which is taken to be equal to 1300°C (the depth of this boundary is determined using the condition of local isostasy).

Alternatively, the distribution of the temperature in an oceanic lithosphere can be calculated with regard to age by the cooling semispace model as follows:

$$\frac{T(z) - T_0}{T(H_L) - T_0} = \mathrm{erf}\left(\frac{z}{2\sqrt{\chi t}}\right), \quad (37)$$

where χ is the thermal conductivity coefficient (accepted to be 10^{-6} m^2/s), erf is the error function, and t is the lithosphere's age.

The depth of the lithosphere bottom is calculated iteratively based on the condition of isostatic equilibrium in each cell of the calculated mesh using the actual data on the relief, thickness, and density of crustal layers, as well as gravitational anomalies in the free air. The algorithm used for the calculation made it possible to determine the temperature distribution by the position of the lithosphere bottom, which in its turn depends on the temperature distribution. We can eliminate this ambiguity by a series of iterations; each of them includes the calculation of the temperature distribution based on the position of the lithosphere bottom, which was calculated in the previous iteration, and the calculation of a new updated depth of the lithosphere bottom.

Calculate the lithosphere's thickness from the rheological profile (Fig. 5) that represents a combination of strength profiles under brittle and plastic conditions [Ranalli, 1995].

The functions of distribution with depth of compression $s_{comp}(z)$ and tension $s_{tens}(z)$ stresses are [Ranalli, 1995; Ershov, 1999; Ershov, Stephenson, 2006] are at a minimum by the absolute value from

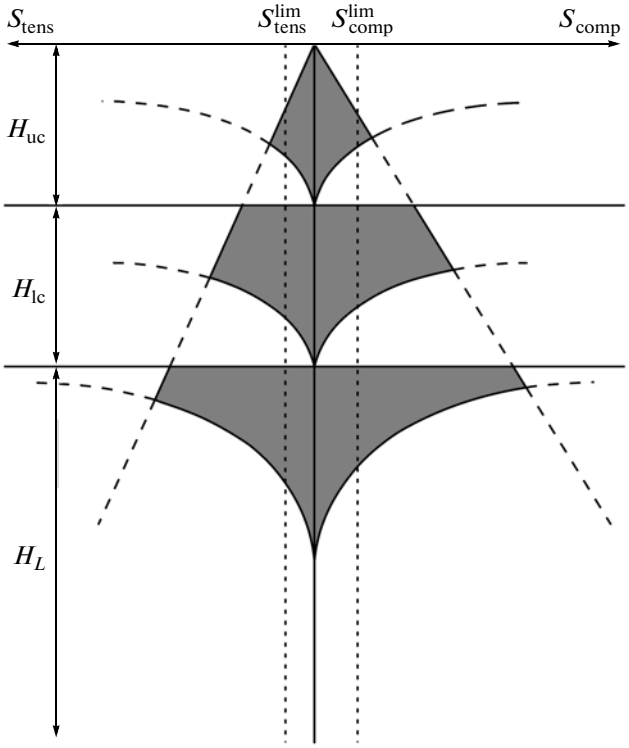

Fig. 5. Rheological profile.

$$s_{yield}(z) = k\rho(z)gz, \quad (38)$$

where $\rho(z)$ is the lithosphere's density, which depends on depth; $s_{yield}(z) = s_{comp}(z)$ at $k = 2$ and $s_{yield}(z) = s_{tens}(z)$ at $k = -0.5$, and

$$s_{yield}(z) = \mathrm{sgn}\left(\dot{\varepsilon}\frac{1}{A_p}\exp\left(\frac{E_p}{RT(z)}\right)\right)^{1/N}, \quad (39)$$

where $\dot{\varepsilon}$, is the strain rate (10^{-14} s^{-1}); R is the universal gas constant (8.32 J/(mol K)), $T(z)$ is the depth depending temperature; A_p, E_p, and N are material constants whose values are presented in the table; and $s_{yield}(z) = s_{comp}(z)$ at sign = 1 and $s_{yield}(z) = s_{tens}(z)$ at sign = -1.

To calculate the lithosphere's compression and tension strengths (σ^{lim}_{comp} and σ^{lim}_{tens}), we need to obtain the integrals $s_{comp}(z)$ and $s_{tens}(z)$ with depth.

1.6. The Principle of Estimating the Difference of the Forces of Gravitational Potential (Generalized Topographic Forces)

Generalized topographic forces refer to tectonic forces that appear due to the presence of inhomogeneities of thicknesses and/or densities of the crustal or mantle layers of the lithosphere. The quantitative estimation of the value of these forces was obtained by the calculation of the

Values of Parameters Used in the Calculations

Parameter	Upper crust	Lower crust	Lithosphere mantle	Measurement unit
Power factor, N	2.72	3.05	3.6	–
Energy of activation, E_p	134	276	530	10^3 J/mole
Near-exponential factor, A_p	6.03×10^{-24}	3.16×10^{-20}	7.2×10^{-18}	$1/\text{sPa}^N$

difference of the gravitational potential of the energy in laterally neighboring regions of the lithosphere [Artyushkov, 1979].

The generalized topographic force in the current node of the calculated mesh was determined as the sum of four vectors, the amplitude of each of them is the difference of the integrals of the lithostatic pressure in the neighboring cells, and the direction is orthogonal to the boundary of the cells. Figure 6 presents the calculation principle for the case of an oceanic lithosphere.

A similar quantitative estimate of gravitational potential due to the influence of the change of its value on the state of the stress in the Earth's lithosphere is shown in the work [Coblentz et al., 1994]. In general, the procedure of their calculation is similar to the procedure described above with two exceptions: first, in this work we calculated only the lithosphere bottom from the principle of local isostasy (the thickness and density of crustal layers were used as the input data), whereas in the work [Coblentz et al., 1994], the depth of a continental and ancient oceanic lithosphere bottom was assigned a constant value (125 km), and the calculated value was the crustal thickness (the densities of the continental and oceanic crust were also assigned constants); second, in the work [Coblentz et al., 1994], the linear thermal model of the lithosphere was accepted at a constant (0°C) temperature on the Earth's surface.

2. THE RESULTS AND THEIR DISCUSSION

The calculated stress field depends on the input parameters of the model (lithosphere properties: density, elastic modules, strength; generalized topographic forces; rheological model of the lithosphere: pure elastic or elasto-plastic). Also the character of the interaction along the boundaries of the lithosphere's plates exerts a great influence on the resulting stress field. We estimated a set of models at different input parameters and conditions on the plate boundaries.

The model quality is determined by the degree of correspondence of the calculated stress field to the observed data. The solution of the inverse problem of obtaining a stress field by the available measuring points is not unique [Galybin and Mukhamediev, 1999;

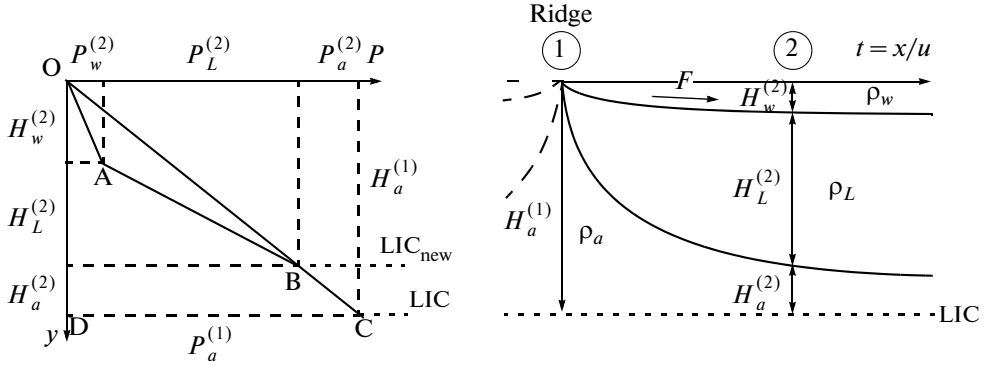

Fig. 6. Fig 6. Principle of calculation of the ridge push force F acting from the ridge (point 1) to point 2. $H_a^{(1)}$ is the thickness of the asthenospherical layer at point 1; $H_w^{(2)}$, $H_L^{(2)}$, and $H_a^{(2)}$ are the thicknesses of the water, lithosphere, and asthenospherical layers at point 2; ρ_w, ρ_L and ρ_a are the densities of the water, lithosphere, and asthenosphere; $P_a^{(1)}$ is the pressure of the asthenospherical column at point 1; $P_w^{(2)}$, $P_L^{(2)}$, and $P_a^{(2)}$ are the pressures of the water, lithosphere, and asthenosphere columns at point 2; LIC- level of isostatic compensation.

Mukha-mediev, 2000; Mukhamediev and Galybin, 2001; Mukha-mediev, et al., 2006]. From this, it follows in general that there may be a whole set of models that are substantially different from each other but that correspond equally well to the actual data.

The measurements from the data base of the international World Stress Map research project were chosen as the actual data and were used for the comparison to determine the quality of the model [Heidbach et al., 2007]. These data are presented in Fig. 7, where the white lines show the projections of the principal axes of elongation on the horizontal plane for the case of normal fault mechanisms and the black lines depict the projections of the principal axes of compression for the case of thrust faults.

The degree of coincidence of strain conditions is usually used as a criterion of correspondence (percentage share of coincidences with respect to the total number of comparable points) or the root-mean-square difference of the angles between the principal axes of the calculated and observed stress tensors [Burbidge, 2004; Liu and Bird, 2002]. This work proposes an alternative criterion. We calculated the root-mean-square deviation of the horizontal components of the calculated and observed stress tensors. This value was averaged for all cells of the calculated mesh with the actual data and was used to estimate the model's quality.

Figure 8 presents the results of the calculations on the continuous uncut mesh, and Figure 9, the model stress field obtained by cutting the mesh along the boundaries of the lithosphere's plates. The spatial position and the geotectonic type of these boundaries are taken in accordance with the data of the digital model by Bird [Bird, 2003]. It is important to indicate that the interaction coefficient (see 1.4) in the model with the cut plates along their boundaries for the regions of continental collision was equal to 1; for the regions of the present spreading, to 0.1; and for the subduction zones, it changed from 0.75 in the regions relative to the low-angle slope slab (for example, the Andian subduction zone) up to 0.25 in the places where the oceanic lithosphere submerges at steeper angles (for example, the Marian subduction zone).

The presented results of the calculations (Figs. 8 and 9) correspond to the best calculated models within the conducted works by the degree of correspondence to the actual data (with respect to the above-described criterion).

The calculated distribution of the stresses of both models that are described in this work is characterized by the following features:

1. The domination of compression stresses within the continents due to the excess of the total compression forces from the adjoining oceanic regions to the continents over the forces of the gravitational spreading of the continents;

2. The domination of compression conditions in the regions of the ancient oceanic lithosphere (20–150 Ma) due to the counter action of forces of ridge push forces and forces of gravitational spreading of the continents;

3. The extension conditions in the regions of the East African–Krasnomorsk rift system and the province of Basins and Ridges due to the action of the forces of sliding down the thermal arch;

4. The extension conditions in the Central Andes and Tibet due to the action of the dominating forces of gravitational spreading over the compression forces.

Despite the fact that both models characterize the main features of the observed stress field rather well, there is a certain difference between them. The main difference of these models from each other is that the model of the continuous lithosphere better exhibits the extension in the middle ridges and adjacent regions of the oceanic lithosphere (0–20 Ma) due to the domination of the ridge push force. The model that accounts for the boundaries of the lithosphere's plates more vividly shows the concentration of stresses in the collision regions (Tibet, Papua New Guinea, New Zealand, and the Alpine belt).

From this it follows that the calculated fields of these two models manifest all the main tectonic structures of the Earth's lithosphere (mid-ocean ridges, subduction zones, intraoceanic rises, continental rift systems, and orogens).

The comparison with the published global models by Bird [Bird, 1998], Lithgow-Bertelloni and Guynn [Lithgow-Bertelloni and Guynn, 2004] shows certain advantages of the models proposed in this work.

The model by Lithgow-Bertelloni and Guynn has the following disadvantages:

1. It does not have explicit tensile stresses directed transversely to the ridge along the Australian–Antarctic, African–Indian and South Pacific ridges;

2. It does not show any signs of the gravitational spreading of the orogens (Tibet and the Andes) and extension in the regions of modern continental rifts (the East African rift system, the province of Basins and Ridges, and Baikal);

3. It exhibits significant tensile stresses within the East European platform, which is not confirmed by the actual data.

As compared with the presented models, the Bird's model has the following features:

1. The extension in the region of the Baikal rift system is not exhibited, and the extensions along the East African–Krasnomorsk rifts do not provide such explicit orientations transversely to their course;

2. Despite the extension within the central part of Tibet, the compressive stresses around its edges are manifested much worse;

3. The extension environment shown for the east of South America does not represent the actual data;

4. On the whole, the extensions along the middle of the ridges are expressed less explicitly.

In general, the model by Bird complies with the actual data much better than the later model by Lithgow-Bertelloni and Guynn, and in some regions, for example, in the west of North and South America, it describes the existing

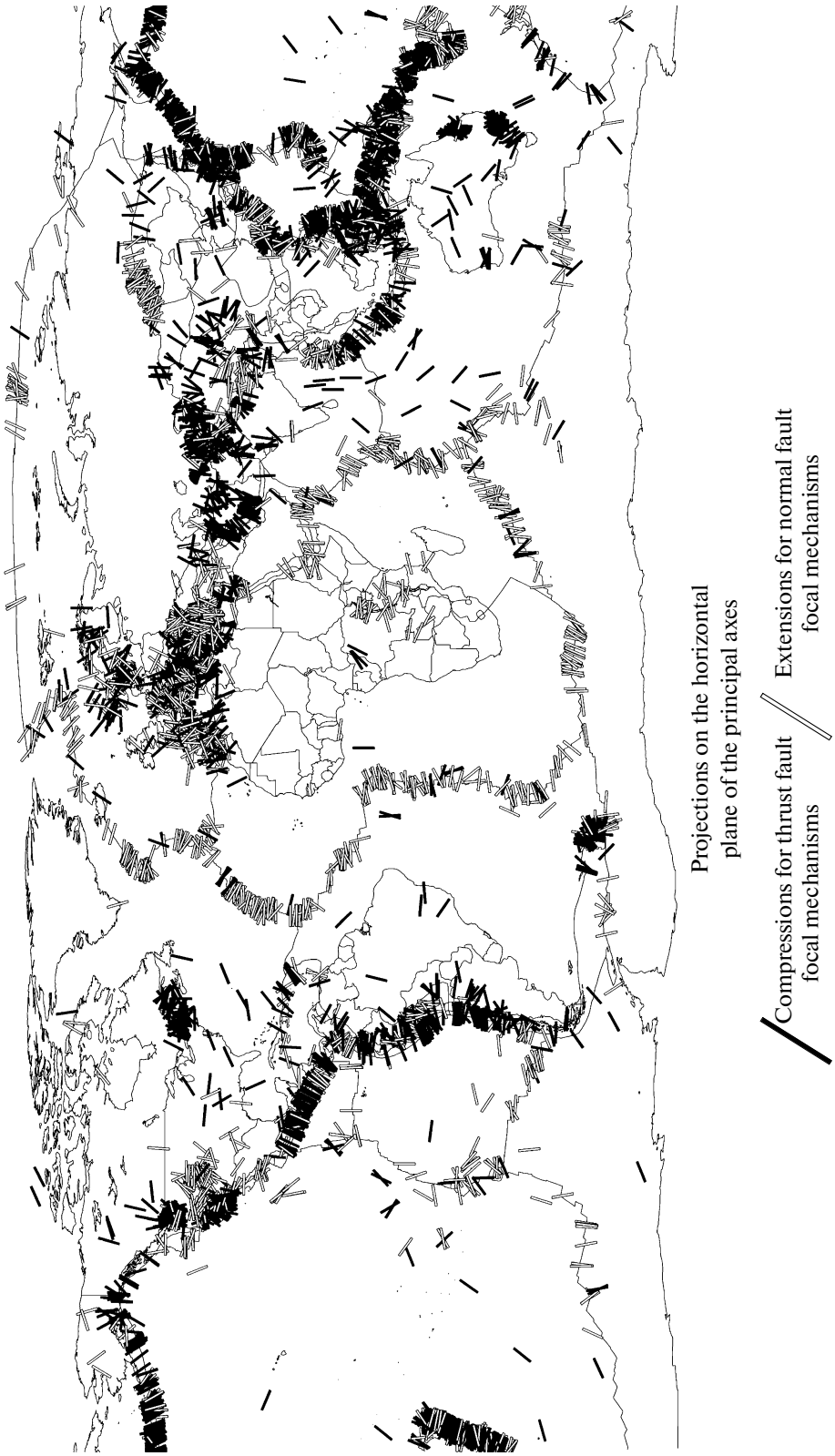

Fig. 7. Distribution of stresses in accordance with the data of the World Stress Map [Heidbach et al., 2007].

Fig. 8. Distribution of stresses that correspond to the best model of the calculated ones at the uncut boundaries of the lithosphere's plates.

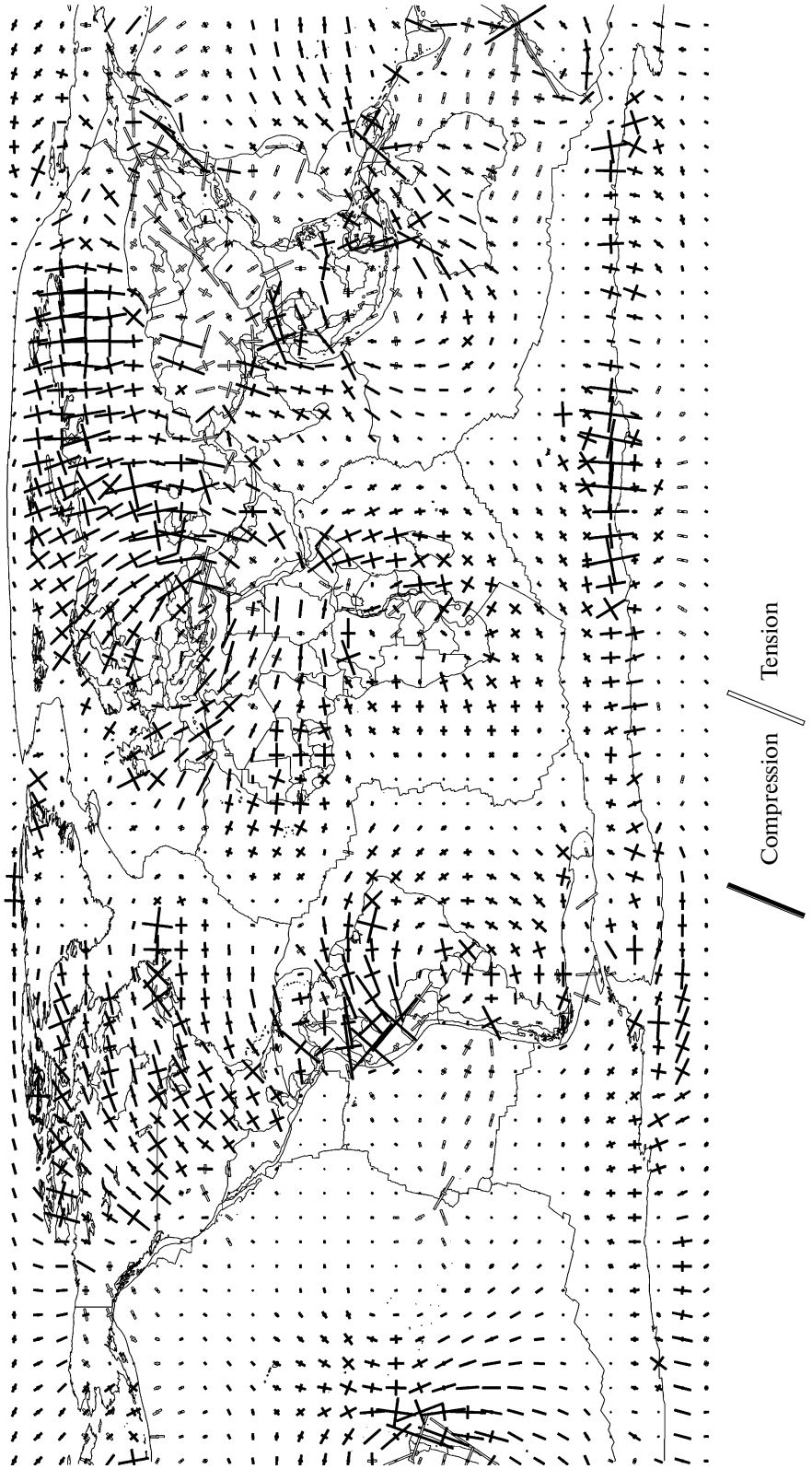

Fig. 9. Distribution of stresses when the boundaries of the lithosphere's plates are cut.

stress field more precisely than the models presented in our work.

Bird, as well as Lithgow-Bertelloni and Guynn indicated that the existing stress field can be explained only by using the mantle forces [Bird, 1998; Lithgow-Bertelloni and Guynn, 2004]. To prove this fact, the stress field was calculated with regard to only topographical forces, and its unsatisfactory correspondence to the actual data was shown. However, our calculations show that the distribution of stresses, that at worst is not inferior to and in some cases exceeds the quality proposed in these models, can be obtained using only the force of the difference of the gravitational potential. The necessity to introduce additional (and quantitatively ambiguously estimated) endogenous forces in the works [Bird, 1998] and [Lithgow-Bertelloni and Guynn, 2004] was probably governed by insufficiently precise calculations of the topographical forces; i.e., the calculations did not take into account all the available and necessary data.

A similar conclusion about the dominant role of the exceeding gravitational potential energy over the other sources in the formation of the stress state in different parts of the Earth's lithosphere was made in the work [Coblentz et al., 1994] based on the good coincidence of moments of generalized topographical forces and actual directions of the rates of movement of the lithosphere's plates at the present time. This work confirms this statement during the same procedure of quantitative estimation of gravitational potential, but unlike the model [Coblentz et al., 1994], the subject of discussion and comparison with the actual data here is no longer the driving force but the tectonic stresses generated by them.

CONCLUSIONS

The original algorithm for the calculation of a two-dimensional stress field of the Earth's lithosphere on a spherical surface is presented. This algorithm is based on the numerical solution of the two-dimensional equation of equilibrium for an elasto-plastic medium by the method of finite volumes using the explicit conservative numerical pattern in the Lagrangian coordinates.

To obtain the lithosphere properties (thermal conditions, elastic modules, density, and strength) and external forces that lead to the formation of the stress field, we used the following set of input data: topography, thicknesses, and the densities of the crustal layers and the upper mantle, gravitational anomalies, the average annual temperature on the Earth's surface, and the rheological and thermal physical properties of the rocks of the lithosphere.

It was accepted that the sources of stresses are only forces of the difference of the gravitational potential (generalized topographical), the slab pull forces and the forces of mantle flows were not included in the model due to the complexity and ambiguity of their precise quantitative estimation.

A comparison between the calculated models and the actual data shows a rather good degree of correspondence of the calculated stress field to the observed one. The calculated stress field reflects all the main structures of the Earth's lithosphere: mid-ocean ridges, zones of continental riftogenesis, present zones of subduction and collisions, as well as large continental orogenes.

The generalized topographical forces depend on the lateral variations of the Earth's surface relief, and on the thickness, structure, and thermal conditions of the lithosphere. Therefore, the quality and details of these data are important for their calculation. The worst degree of correspondence to the actual data of the previously published models that take into account topographical forces is caused by incomplete and insufficient details of the input data of these models.

The results of this work can dispute the results of the earlier published works on modeling the global stress field that point to the necessity of using forces of mantle flows in the calculations. The higher degree of correspondence of the results of our modeling to the actual data indicates that the determining role in the formation of a modern stress field is played by the forces of the difference of the gravitational potential (generalized topographical forces).

Thus, in accordance with the results of our modeling we can conclude that when the generalized topographical forces are calculated correctly and sufficiently fully, they can generate a stress field that corresponds to the observed one and that can explain tectonic structures of the first order.

REFERENCES

National Geophysical Data Center. ETOPO-5 Bathymetry and Topography Data, in Data Announc. 88-MGG-02, NOAA, Boulder, Col., 1988.

Artyushkov, E.V., Geodinamika (Geodynamics), Moscow: Nauka, 1979.

Artyushkov, E.V., Stresses in the Lithosphere Caused by Crustal Thickness Inhomogeneities, *J. Geophys. Res.*, 1973, vol. 78, pp. 7675–7708.

Bassin, C., Laske, G., and Masters, G., The Current Limits of Resolution for Surface Wave Tomography in North America, EOS Trans AGU, 2000, vol. 81, p. F897.

Bird, P., An Updated Digital Model of Plates Boundaries, Geochem., Geophys., Geosystems. *An Electronic Journal of the Earth Sciences,* vol. 4, no. 3, p. 14, 2003.

Bird, P., Testing Hypotheses on Plate-Driving Mechanisms with Global Lithosphere Models Including Topography, Thermal Structure, and Faults, *J. Geophys. Res.*, 1998, vol. 103, p. 129.

Burbidge, D.R., Thin Plate Neotectonic Models of the Australian Plate, *J. Geophys. Res.*, 2004, vol. 109.

Coblentz, D. and Sandiford, M., Tectonic Stresses in African Plate: Constraints on the Ambient Lithospheric Stress State, Geology, 1994, vol. 22, pp. 831–834.

Coblentz, D.D. and Richardson, R.M., Analysis of the South American Intraplate Stress Field, *J. Geophys. Res.*, 1996, vol. 101, pp. 8643–8657.

Coblentz, D.D., Richardson, R.M., and Sandiford, M., On the Gravitational Potential of the Earth's Lithosphere, Tectonics, 1994, vol. 13, pp. 929–945.

Coblentz, D.D., Sandiford, M., Richardson, R.M., Zho, S., and Hillis, R., The Origins of the Intraplate Stress Field in Continental Australia, Earth Planet. *Sci. Lett.*, 1995, vol. 133, pp. 299–309.

Coblentz, D.D., Zhou, S., Hillis, R.R., Richardson, R.M., and Sandiford, M., Topography, Boundary Forces, and the Indo-Australian Intraplate Stress Field, *J. Geophys. Res.*, 1998, vol. 103, pp. 919–931.

Ershov, A.V., Reologiya litosfery. V: *Geoistoricheskii i geodinamicheskii analiz osadochnykh basseinov* (Rheology of Lithosphere. In: Geohistorical and Geodynamical Analysis of Sedimentary Basins), Moscow: MPR RF, 1999.

Ershov, A.V. and Stephenson, R.A., Implications of a Visco-Elastic Model of the Lithosphere for Calculating Yield Strength Envelopes, J. of Geodynamics, 2006, vol. 42, pp. 12–27.

Flesch, L.M., Holt, W.E., Haines, A.J., and Shen-Tu, B., *Dynamics of the Pacific-North American Plate Boundary in the Western United States, Scienc*e, 2000, vol. 287, pp. 834–836.

Forsyth, D. and Uyeda, S., On the Relative Importance of the Driving Forces of Plate Motion, Geophys. *J.R. Astron. Soc*, 1975, vol. 43, pp. 163–200.

Frank, F.C., Plate Tectonics, the Analogy with Glacier Flow, and Isostasy, in Flow and Fracture of Rocks, *Geophys. Monogr. Ser,* 1972, vol. 16, pp. 285–292.

Galybin, A.N. and Mukhamediev, Sh.A., Plane Elastic Boundary Value Problem Posed on Orientation of Principal Stresses, *J. Mech. Phys. Solids,* 1999, vol. 47, pp. 2381–2409.

Harper, J.R., On the Driving Forces of Plate Tectonics, *Geophys. J. R. Astron Soc*, 1975, vol. 40, pp. 465–474.

Heidbach, O., Fuchs, K., Muller, B., Reinecker, J., Sperner, B., Tingay, M., and Wenzel, F., Eds., The World Stress Map—Release 2005 (Commission for the Geological Map of the World), Paris, 2007.

Kochin, N.E., *Vektornoe ischislenie i nachala tenzornogo ischisleniya* (Vector Analysis and Principles of Tensor Calculation), Moscow: Nauka, 1965.

Leemans, R. and Cramer, W., *The IIASA database for Mean Monthly Values of Temperature, Precipitation and Cloudiness* on a Global Terrestrial Grid. Research Report RR-91-18 (Int. Inst. of Appl. Syst. Analysis), Laxenburg, 1991, p. 61.

Lemoine, F.G., Kenyon, S.C., Factor, J.K., Trimmer, R.G., Pavlis, N.K., Chinn, D.S., Cox, C.M., Klosko, S.M., Luthcke, S.B., Torrence, M.H., Wang, Y.M., Williamson, R.G., Pavlis, E.C., Rapp, R.H., and Olson, T.R., *The Development of the Joint NASA GSFC and NIMA Geopotential Model EGM96*, NASA Goddard Space Flight Center, Greenbelt, Md., 1998.

Lieth, H., Modelling the Primary Productivity of the Earth. Nature and Resources, in *UNESCO, VIII, 2:5–10*, 1972.

Lithgow-Bertelloni, C. and Guynn, J., Origin of the Lithospheric Stress Field, *J. Geophys. Res.*, 2004, vol. 109.

Liu, Z. and Bird, P., Computer Simulation of Neotectonics in Latitudes 22-70, Western North America (Abstract), *Eos Trans. AGU, Fall Meet. Suppl.*, 1998, vol. 79, p. F566.

Liu, Z. and Bird, P., Finite Element Modeling of Neotectonics in New Zealand, *J. Geophys. Res.*, 2002, vol. 2328, no. B12.

Meijer, P.T., Govers, R., and Wortel, M.J.R., Forces Controlling the Present-Day State of Stress of the Andes, *Earth Planet. Sci. Lett.*, 1997, vol. 148, pp. 157–170.

Mooney, A., Laske, G., and Masters, G., Crust 5.1: a Global Crustal Model at 5 x5 Degrees, *J. Geophys. Res.,* 1998, vol. 103, pp. 727–747.

Mukhamediev, Sh.A., Neklassicheskie kraevye zadachi mekhaniki sploshnoi sredy dlya geodinamiki, *Dokl. Akad. Nauk*, 2000, vol. 373, no. 2, pp. 242–246 [*Dokl.* (Nonclassical Boundary Problems of Continuous Medium Mechanics for Geodynamics), vol. 373, no. 2, pp.].

Mukhamediev, Sh.A. and Galybin, A.N., *Pryamoi podkhod k opredeleniyu regional'nykh polei napryazhenii (na primere Zapadno-Evropeiskoi, Severo-Amerikanskoi i Avstraliiskoi platform)*, *Fiz. Zemli*, 2001, no. 8, pp. 23–41.

Mukhamediev, Sh.A., Galybin, A.N., and Brady, B.H.G., Determination of the Stress Fields in the Elastic Lithosphere by Methods Based on the Stress Orientations *Int. J. of Rock Mechanics and Mining Sciences*, 2006, vol. 43, pp. 66–88.

Pacanovsky, K., Davis, D., Richardson, R., and Coblentz, D., Interplate Stresses and Plate-Driving Forces in the Philippine Sea Plate, *J. Geophys. Res.,* vol. 104, no. B1, pp. 1095–1110.

Poliakov, A., Cundall, P., Podladchikov, Yu., and Lyakhovsky, V., An Explicit Inertial Method for the Simulation of Viscoelastic Flow: An Evaluation of Elastic Effects on Diapiric Flow in Two and Three Layer Models, *Proc. of NATO Advanced Study Institute on Dynamic Modeling and Flow in the Earth and Planets, Stone D.B and Runcorn S.K., Eds. Flow and Creep in the Solar System: Observations, Modeling and Theory*, Kluwer, Holland, 1993, pp. 175–195.

Ranalli, G., *Rheology of the Earth*, 2nd ed.,Chapman & Hall, 1971, p. 407.

Reynolds, S.D., Coblentz, D.D., and Hillis, R.R., Tectonic Forces Controlling the Regional Intraplate Stress Field in Continental Australia: Results from New Finite Element Modeling, *J. Geophys. Res.*, 2002, vol. 107, no. B7.

Richardson, R. and Reding, L., North American Plate Dynamics, *J. Geophys. Res.*, 1991, vol. 96, no. B7, pp. 12.201–12.223.

Richardson, R.M., Solomon, S.C., and Sleep, N.H., Intraplate Stress as an Indicator of Plate Tectonic Driving Forces, *J. Geophys. Res.*, 1976, vol. 81, pp. 1847–1856.

Richardson, R.M., Solomon, S.C., and Sleep, N.H., Tectonic Stress in the Plates, *Rev. Geophys.*, 1979, vol. 17, pp. 981–1019.

Sandiford, M., Coblentz, D., and Richardson, R., Ridge Torques and Continental Collision in the Indian-Australian Plate, *Geology*, 1995, vol. 23, no. 7, pp. 653–656.

Solomon, S.C., Sleep, N.H., and Richardson, R.M., On the Forces Driving Plate Tectonics: Inferences from Absolute Plate Velocities and Intraplate Stress, *Geophys. J. R. Astr. Soc.*, 1975, vol. 42, pp. 769–801.

Uyeda, S., *The New View of the Earth*, San Francisco: W.H. Freeman, 1978.